Interactions between a magnon mode and a cavity photon mode mediated by traveling photons

J. W. Rao,[1,2,*] Y. P. Wang,[1] Y. Yang,[1] T. Yu,[3] Y. S. Gui,[1] X. L. Fan,[2] D. S. Xue,[2] and C.-M. Hu[1,†]

[1]*Department of Physics and Astronomy, University of Manitoba, Winnipeg, Canada R3T 2N2*

[2]*The Key Lab for Magnetism and Magnetic Materials of Ministry of Education, Lanzhou University, Lanzhou 730000, China*

[3]*Kavli Institute of NanoScience, Delft University of Technology, 2628 CJ Delft, The Netherlands*

(Received 11 December 2019; revised manuscript received 23 January 2020; accepted 23 January 2020; published 5 February 2020)

We systematically study the indirect interaction between a magnon mode and a cavity photon mode mediated by traveling photons of a waveguide. From a general Hamiltonian, we derive the effective coupling strength between two separated modes, and obtain the theoretical expression of the system's transmission. Accordingly, we design an experimental setup consisting of a shield cavity photon mode, a microstrip line, and a magnon system to test our theoretical predictions. From measured transmission spectra, indirect interaction, as well as mode hybridization, between two modes can be observed. All experimental observations support our theoretical predictions. In this work we clarify the mechanism of traveling photon mediated interactions between two separate modes. Even without spatial mode overlap, two separated modes can still couple with each other through their correlated dissipations into a mutual traveling photon bus. This conclusion may help us understand the recently discovered dissipative coupling effect in cavity magnonics systems. Additionally, the physics and technique developed in this work may benefit us in designing new hybrid systems based on the waveguide magnonics.

DOI: 10.1103/PhysRevB.101.064404

I. INTRODUCTION

Engineering hybrid systems which combine complementary physical components is one of the central goals in quantum technology [1–5]. Following this approach in the past few years, the field of cavity magnonics has been developed through the coupling of collective spin excitations, i.e., magnons, with cavity photons [6,7]. This system was first proposed by Soykal and Flatté in 2010 [7], but only realized experimentally since 2013 [8–15]. So far, many technologies have been developed based on this versatile system, for example the gradient memory architecture [16], single magnon detection [17], nonlocal spin current manipulation [18], cavity magnon polariton logic gate [19], giant nonreciprocity [20], etc. In all these previous works, spatial mode overlap between the cavity microwave field and the magnon mode is essential to achieve strong photon-magnon interaction, and hence magnon systems are deliberately placed inside cavities. An inevitable problem is that all operations in cavity magnonics systems must take in account both the geometry and mode distribution of cavities. To get rid of these spatial limitations, coupling a magnon system to other resonant components, including cavity photon, qubit, and atom, etc., through traveling photons may be a feasible solution.

In fact, this kind of indirect interactions mediated by traveling photons is the main object of research in waveguide quantum electrodynamics (QED). It has been verified in various systems including quantum dots [21,22], atoms [23–25], and superconducting circuits [26–28], but has not yet been tested in a magnon system. In this work, we first extend the idea of waveguide QED into the magnon system, and systematically study the interaction between a magnon mode and a separated cavity photon mode. At the beginning we construct a general Hamiltonian from which a theoretical explanation of the indirect interaction between two separated modes is given. This effect is sustained by traveling photons, and its intensity equals the square root of the product of the two modes' phase correlated dissipations. Accordingly, we design an experimental setup consisting of a magnon system, microstripline, and a shield cavity photon mode. From a measured transmission spectra, mode hybridization between the magnon mode and the separated cavity photon mode can be observed, which exhibits a strong dependency in the separation of the two modes. All these experimental observations well confirm our theoretical predictions. Our work clarifies the mechanism of dissipative coupling mediated by traveling photons, which is useful for us to understand the recently discovered dissipative coupling [20,29–37] and giant nonreciprocity [20] in cavity magnonics systems. Additionally, the physics and technique developed in our work may help us design a new hybrid system based on waveguide magnonics.

II. THEORETICAL MODEL

In cavity magnonics systems, strong interactions between a cavity photon and a magnon arise from the spatial overlap of the cavity microwave field and the magnon mode. However, in a waveguide magnonics system, such a direct overlap is unnecessary, because a magnon mode in the waveguide can be coupled to other components, including a separated cavity photon mode, through their correlated dissipations into a mutual waveguide photon bus.

*jinweir@myumanitoba.ca
†Can-Ming.Hu@umanitoba.ca

A. A general Hamiltonian for the waveguide magnonics

To illustrate this effect, we construct a general Hamiltonian in the form of

$$H = \hbar\widetilde{\omega}_m \hat{m}^\dagger \hat{m} + \hbar\widetilde{\omega}_a \hat{a}^\dagger \hat{a} + \int \hbar\omega_k \hat{p}_k^\dagger \hat{p}_k dk + \int \hbar[\lambda_m e^{i\phi}(\hat{m} + \hat{m}^\dagger)(\hat{p}_k + \hat{p}_k^\dagger) + \lambda_a(\hat{a} + \hat{a}^\dagger)(\hat{p}_k + \hat{p}_k^\dagger)]dk, \quad (1)$$

where $\hat{m}(\hat{m}^\dagger)$ and $\hat{a}(\hat{a}^\dagger)$ are the annihilation (creation) operators of the magnon mode, such as the uniform Kittel mode, and the other resonant mode, respectively. $\widetilde{\omega}_m$ and $\widetilde{\omega}_a$ correspond to their uncoupled mode frequencies, which are complex and defined as $\widetilde{\omega}_m = \omega_m - i\alpha$ and $\widetilde{\omega}_a = \omega_a - i\beta$. α and β, respectively, represent the intrinsic damping rates of the two modes. Considering these two modes are separated from each other in a waveguide, there is no direct mode overlap between them. Therefore, the direct coupling effect between them has not been considered in this Hamiltonian. The third term of the Hamiltonian represents traveling photons in a waveguide, which is an integral of wave vector over the whole real domain ($-\infty$ to ∞). $\hat{p}_k$ is the boson annihilation operator of the traveling photon with $[\hat{p}_k, \hat{p}_{k'}] = \delta(k - k')$. ω_k is the frequency of the traveling photon with a wave vector of k. The last term of the Hamiltonian describes the dipole interactions between traveling photons and each mode, which are linear in $\hat{p}_k$ and $\hat{p}_k^\dagger$. λ_m and λ_a are individual coupling strengths of the two modes with traveling photons, which arise from the mode overlap between the magnon/cavity mode and the traveling photons. ϕ indicates the phase delay of the traveling photon from one mode to another, i.e., $\phi = kL$, where L is the separation between the two modes. Because our following study is mainly focused on the interactions between two separated modes near the zero-detuning condition, i.e., $\omega_a \approx \omega_m$, we can simply assume that ϕ is a constant for different k.

B. Derivation of the Langevin equations

Following a standard procedure [38–40] and using the rotation-wave approximation, the equation of motion for the traveling photon $\hat{p}_k$ can be solved from Eq. (1):

$$\frac{d\hat{p}_k}{dt} = -\frac{i}{\hbar}[\hat{p}_k, H] = -i\omega_k \hat{p}_k - i\lambda_m e^{i\phi}\hat{m} - i\lambda_a \hat{a} \quad (2)$$

leading to

$$\hat{p}_k(t) = e^{-i\omega_k(t-t_0)}\hat{p}_k(t_0) - \int_{t_0}^{t} i[\lambda_m e^{i\phi}\hat{m} + \lambda_a \hat{a}]e^{-i\omega_k(t-t')}dt', \quad (3)$$

where $\hat{p}_k(t_0)$ is $\hat{p}_k$ at the initial time of t_0 ($t_0 < t$). Also from the Eq. (1), motion equations of the magnon mode and the other mode can be solved as

$$\frac{d\hat{m}}{dt} = -i\widetilde{\omega}_m \hat{m} - \int i\lambda_m e^{i\phi}\hat{p}_k dk,$$
$$\frac{d\hat{a}}{dt} = -i\widetilde{\omega}_a \hat{a} - \int i\lambda_a \hat{p}_k dk. \quad (4)$$

According to the first Markov approximation, $\lambda_{a,m}$ can be treated as constants, so that both of them can be put outside the integral over k. Substituting Eq. (3) into Eq. (4), the derived quantum Lagevin equations of the two modes are

$$\frac{d\hat{m}}{dt} = -i\widetilde{\omega}_m \hat{m} - 2\pi\left(\lambda_m^2 \hat{m} + \lambda_m \lambda_a e^{i\phi}\hat{a}\right) - i\sqrt{2\pi}\lambda_m e^{i(\phi+\theta)}\hat{p}^{\text{in}},$$
$$\frac{d\hat{a}}{dt} = -i\widetilde{\omega}_a \hat{a} - 2\pi\left(\lambda_a^2 \hat{a} + \lambda_m \lambda_a e^{i\phi}\hat{m}\right) - i\sqrt{2\pi}\lambda_a \hat{p}^{\text{in}}. \quad (5)$$

Here, damping terms depend only on the two modes' operators evaluated at time t. In addition, considering that both modes are two-side systems with mirror-symmetry boundaries, their damping rates induced by traveling photons have been doubled in Eq. (5) [39]. $\hat{p}^{\text{in}}$ is the input field which is defined as

$$\hat{p}^{\text{in}}(t) = \frac{1}{\sqrt{2\pi}} \int e^{-i\omega_k(t-t_0)}\hat{p}_k(t_0)dk. \quad (6)$$

In our assumptive system, the two modes are separately placed in a waveguide. Input field ($\hat{p}^{\text{in}}$) arrives at each position at a different time. Such a time delay has been considered by a traveling phase ϕ. In addition, besides this delay, the phase shift of an input field after passing through a resonant mode should also be considered. For instance, an input field passes through the mode $\hat{a}(\hat{a}^\dagger)$ first before arriving at the magnon mode. The phase of input field ($\hat{p}^{\text{in}}$) would be delayed by zero at $\omega_k \ll \omega_a$, 90° at $\omega_k = \omega_a$ and 180° at $\omega_k \gg \omega_a$. In Eq. (5), this resonant phase delay [41] is described by θ.

Radiative damping rates of the two modes are approximately defined as $\gamma \approx 2\pi\lambda_m^2$ and $\kappa \approx 2\pi\lambda_a^2$, respectively. Substituting them into Eq. (5), we get

$$\frac{d}{dt}\begin{bmatrix}\hat{m}\\ \hat{a}\end{bmatrix} = -i\begin{bmatrix}\omega_m - i(\alpha+\gamma) & -i\sqrt{\kappa\gamma}e^{i\phi}\\ -i\sqrt{\kappa\gamma}e^{i\phi} & \omega_a - i(\beta+\kappa)\end{bmatrix}\begin{bmatrix}\hat{m}\\ \hat{a}\end{bmatrix} - i\begin{bmatrix}\sqrt{\gamma}e^{i(\phi+\theta)}\\ \sqrt{\kappa}\end{bmatrix}\hat{p}^{\text{in}}(t). \quad (7)$$

Unlike the two aforementioned radiative damping rates, these two intrinsic damping rates have no effect on the interactions between the two modes. They correspond to the inelastic scattering process of the two resonant modes, and dissipate the modes' energies into the surroundings as heat. According to our theoretical model, the coupling strength between these two separated modes is $-i\sqrt{\kappa\gamma}e^{i\phi}$. Obviously, when $\phi = n\pi$ ($n = 0, 1, 2, 3, \ldots$), it becomes an imaginary number, i.e., the coupling effect between the two modes is purely dissipative.

C. Transmission spectrum of the system

From Eq. (2), if we consider $t_1 > t$, traveling photon $\hat{p}_k$ after interacting with the two modes is

$$\hat{p}_k(t) = e^{-i\omega_k(t-t_1)}\hat{p}_k(t_1) + \int_{t}^{t_1} i[\lambda_m e^{i\phi}\hat{m} + \lambda_a \hat{a}]e^{-i\omega_k(t-t')}dt'. \quad (8)$$

The output field is defined as

$$\hat{p}^{\text{out}}(t) = \frac{1}{\sqrt{2\pi}} \int e^{-i\omega_k(t-t_1)}\hat{p}_k(t_1)dk. \quad (9)$$

Carrying on the same procedures of Eqs. (4)–(7), the time-reversed Langevin equation of the system can be derived,

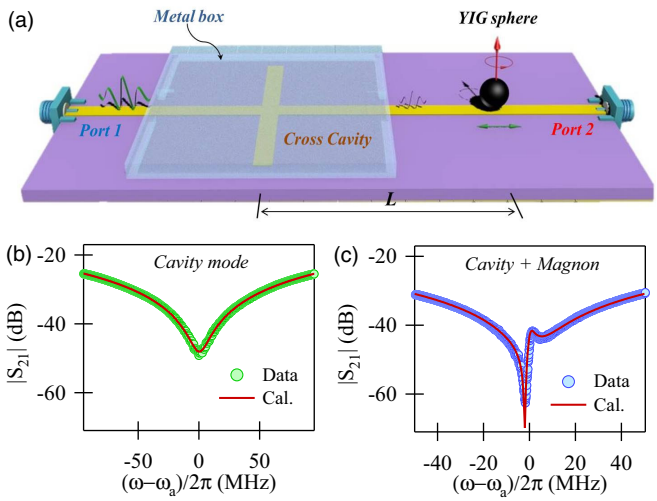

FIG. 1. (a) Schematic diagram of the experimental setup. The cross cavity is shielded by a metal box, so that it can only interact with the magnon mode via the transmission line. The experiment setup is placed in an electromagnet. The bias magnetic field produced by the electromagnet is perpendicular to the plane of the cross cavity. (b) Without the YIG sphere, the measured (green dots) and calculated (red solid line) transmission spectrum of the system. (c) At the condition of $\omega_m = \omega_a$, the measured (blue dots) and calculated (red solid line) transmission spectrum.

which describes the relation between two separated modes and the output field $\hat{p}^{\text{out}}$. Combining it with Eq. (7), we can obtain the input-output relation of the system as

$$\hat{p}^{\text{out}}(t) = \hat{p}^{\text{in}}(t) - i[\sqrt{\gamma}e^{i(\phi+\theta)}\hat{m} + \sqrt{\kappa}\hat{a}]. \tag{10}$$

Using Eqs. (7) and (10), the transmission spectrum of the system can be solved as

$$S_{21} = \frac{\langle \hat{p}^{\text{out}} \rangle}{\langle \hat{p}^{\text{in}} \rangle} = 1 - i(\sqrt{\gamma}e^{i(\phi+\theta)}, \sqrt{\kappa}) \times \begin{bmatrix} \omega - \widetilde{\omega}_{m'} & i\sqrt{\kappa\gamma}e^{i\phi} \\ i\sqrt{\kappa\gamma}e^{i\phi} & \omega - \widetilde{\omega}_{a'} \end{bmatrix}^{-1} \begin{bmatrix} \sqrt{\gamma}e^{i(\phi+\theta)} \\ \sqrt{\kappa} \end{bmatrix}, \tag{11}$$

where $\widetilde{\omega}_{m'}$ and $\widetilde{\omega}_{a'}$, respectively, represent the two modes' complex frequencies, i.e., $\widetilde{\omega}_{m'} = \omega_m - i(\alpha + \gamma)$ and $\widetilde{\omega}_{a'} = \omega_a - i(\beta + \kappa)$. Because the transmission spectrum can be directly measured from experiment, we choose it as the main study object in our following experiments. From Eq. (11) we note that transmission spectrum is a mixture of two different effects. Besides the indirect coupling effect with a strength of $-i\sqrt{\kappa\gamma}e^{i\phi}$, interference between two channels of input field $\hat{p}^{\text{in}}$ via $\sqrt{\gamma}e^{i(\phi+\theta)}$ and $\sqrt{\kappa}$ also exists.

III. EXPERIMENTAL RESULTS

A. Characterization of the indirectly coupled cavity magnon system

Based on the theoretical model, we designed an experiment to test the indirect interaction between a magnon mode and a cavity photon mode in a planar waveguide. Figure 1(a) shows the experimental setup, which contains three main parts: (i) a cross cavity, which is shielded by a metal box; (ii) a yttrium iron garnet sphere (YIG), whose position can be precisely controlled by a motor stage; and (iii) a 50 Ohm matched microstrip line, which is used to connect the cross cavity and the YIG sphere. In experiment, to achieve a strong coupling effect, the uniform Kittel mode of the YIG sphere is chosen, because it has the most spins to couple with the traveling photons. The uniform Kittel mode follows the dispersion $\omega_m = \gamma(H + H_A)$, where $\gamma = 2\pi \times 26.3\ \mu_0\,\text{GHz/T}$ is the gyromagnetic ratio, $H_A = -1.3$ mT is magnetocrystalline anisotropy field, and H is the static bias magnetic field applied perpendicular to the cross cavity.

The impedance matched microstrip line is fabricated on a 0.813-mm-thick RO4003C substrate with a width of 1.67 mm. The cross cavity consists of two perpendicular arms, and is conductively connected to the microstrip line. The half-length of its vertical arm is 17.5 mm, which determines the mode frequencies of the cavity. A 1-mm-diameter YIG sphere is placed on the top of the microstrip line and away from the cavity photon mode. A motor stage is used to move the YIG sphere along the microstrip line, and its variation range is from $L = 25$ mm to $L = 60$ mm. Because the cavity photon mode is shielded by the metal box, no direct mode overlap exists between it and the magnon mode. Considering both of these modes are coupled to a mutual transmission line, any interaction arising between them can be attributed to the mediation of traveling photons.

Without the YIG sphere, the transmission spectrum (S_{21}) of the system is plotted in Fig. 1(b) as a function of $\Delta_a = \omega - \omega_a$. From it, radiative damping rate ($\kappa/2\pi$), intrinsic damping rate ($\beta/2\pi$), and mode frequency ($\omega_a/2\pi$) of the cross cavity are fitted as 1.77 GHz, 7 MHz, and 2.775 GHz, respectively. The red solid line is the calculation result by using Eq. (11) with setting $\omega_m/2\pi = 0$ GHz. After placing a YIG sphere at $L = 41$ mm [Fig. 1(a)] and setting $\omega_a = \omega_m$, the measured transmission spectrum of the system is plotted in Fig. 1(c). The two resonant dips in the spectrum are the result of the hybridization of the cavity photon mode and the magnon mode. Besides a small dip at $\Delta_a/2\pi = 4$ MHz, an ultrasharp dip [20,42] occurs at $\Delta_a/2\pi = -3$ MHz with an amplitude of nearly -70 dB. Still using Eq. (11), this spectrum can be well reproduced [red solid line in Fig. 1(c)] with setting $\gamma/2\pi = 0.58$ kHz, $\alpha/2\pi = 1.38$ MHz, $\phi = 40.3°$, and $\theta = 90°$. In this case, $\theta = 90°$ is because mode hybridization was measured at the condition of $\omega_a = \omega_m$. After passing through the cavity mode, the phase of input signal (p^{in}) would be shifted by 90°.

B. Indirect interaction between two separate modes at different separations

After characterizing the system, we set $\omega_m = \omega_a$, and the measure transmission spectra of the system at different positions of YIG sphere. Figure 2(a) shows the results in which transmission are plotted as a function of Δ_a and the separation (L). The yellow color represents the aforementioned ultrasharp resonant dip, which occurs from $-\Delta_a$ to $+\Delta_a$ with increasing the separation L, and nearly disappears at $L = 47$ mm. Figures 2(b)–2(d) are three typical spectra, respectively, measured at $L = 53$ mm, $L = 47$ mm, and $L = 41$ mm. By using Eq. (11), all these three spectra have been well described (red solid lines).

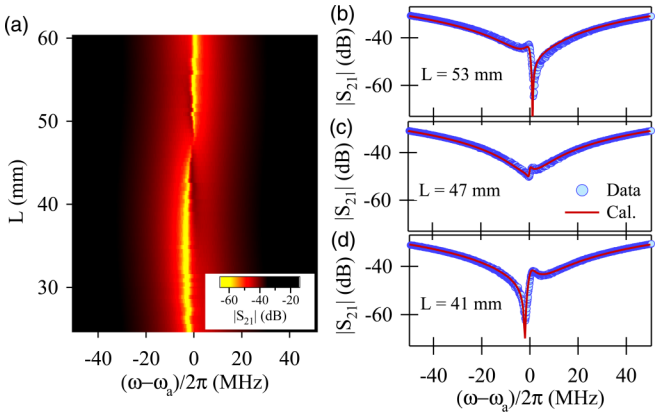

FIG. 2. (a) Transmission of the system ($|S_{21}|$) as a function of Δ_a and the separation between the two modes L. (b)–(d) Three typical spectra measured at $L = 53$ mm, $L = 47$ mm, and $L = 41$ mm. Blue dots are experimental data and red solid lines are calculation results by using Eq. (11).

Furthermore, we fit all spectra shown in Fig. 2(a), and plot the results in Figs. 3(a)–3(c). The radiative damping rate γ decreases from maximum to zero, and then becomes negative after $L = 47$ mm [Fig. 3(a)]. By contrast, the intrinsic damping rate of the magnon mode α [Fig. 3(b)] shows a sinusoidal dependence in separation L. It reaches the maximal value at $L = 30$ mm, and then decreases to a minimal value at $L = 47$ mm. As indicated by two dashed lines in Figs. 3(a) and 3(b), the separation between the maximal and minimal values of the intrinsic damping rate is 17 mm, which approximately equals the half-length of the vertical arm of cross cavity (17.5 mm), i.e., a quarter wavelength of cavity photon mode [26,27]. Such consistency between the spatial variation of damping rates and the wavelength of the cavity

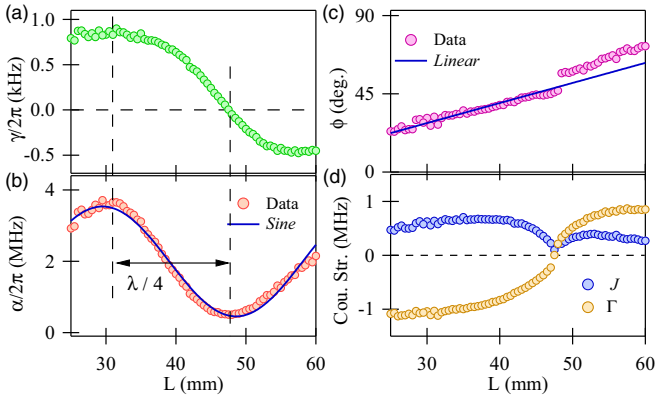

FIG. 3. (a) and (b) Radiative damping rate (γ) and intrinsic damping rate (α) of the magnon mode fitted from transmission spectra shown in Fig. 2(a). A sine function [blue solid line in (b)] is plotted to guide the eyes. The separation between the maximal and minimal values of the two damping rates is indicated by two dashed lines, which equals a quarter wavelength of cavity photon mode. (c) Relative phase (ϕ) as a linear function of the separation L. (d) Effective coherent coupling strength J and dissipative coupling strength Γ at different separations L.

photon mode indicates the influence on the magnon system from the separate cavity photon mode.

In our system, the magnon mode interacts with traveling photons, which leads to relaxation, due to the emission of a photon at the resonant frequency, and a Lamb shift of mode frequency, due to the emission of virtual photons. Since both real and virtual photons can travel for a long distance in a transmission line before being lost, they have a chance to be absorbed by the separate cavity photon mode when passing through it [26,27]. Likewise, the inverse process from cavity photon mode to the magnon mode is also true. Because of the exchange of real and virtual photons through a mutual transmission line, a nontrivial interaction between two separate modes arises. For the magnon mode, it emits photons to the transmission line, and, meanwhile, absorbs photons transmitted from the cavity photon mode. The residue of these two competitive processes results in the radiative damping of the magnon mode (γ). Depending on which process is dominant, the radiative damping of the magnon mode can be either positive or negative, as shown in Fig. 3(a). At $L =$ 47 mm, because the two processes nearly cancel each other, the radiative damping rate of the magnon mode vanishes.

Additionally, for the spatial variation of intrinsic damping rate α, we conjecture it may arise from the inelastic scattering process of the magnon mode. α contains two main parts: Gilbert damping and inelastic radiation. Gilbert damping of the magnon mode is determined by the material's properties, which is independent of YIG's position. By contrast, the inelastic radiation of the magnon mode relates to the redistribution of the waveguide electromagnetic field because of the existence of the cavity photon mode. When γ reaches the maximal value at $L = 30$ mm, energy dissipation of the magnon mode into both the traveling wave and the cavity photon mode reaches the maximal. Consequently, inelastic radiation of the magnon mode is enhanced, and α reaches its maximal value at this position. However, at $L = 47$ mm, both two dissipation channels are shut down, because γ nearly vanishes. In this condition, the magnon mode becomes decoupled with its surroundings [26], so that inelastic radiation of the magnon mode nearly disappears. α falls back to the Gilbert damping rate around 0.5 MHz [43].

Unlike the two damping rates of the magnon mode, the traveling phase (ϕ) exhibits a good linear relation with the separation L. Based on experimental data, ϕ at $L = 0$ mm can be calculated as $-5^\circ (\approx 0^\circ)$, which indicates coupling strength $-i\sqrt{\kappa\gamma}e^{i\phi}$ is an imaginary number at the intersection of the cross. In this condition, the coupling effect between the two modes is purely dissipative. This conclusion derived from our theoretical model is well consistent with previous works performed in the cross cavity [20,32].

By using the extracted γ and ϕ from curve fitting, the effective coupling strength between two separated modes, i.e., $-i\sqrt{\kappa\gamma}e^{i\phi} = J + i\Gamma$, can be calculated [Fig. 3(d)]. Here J and Γ, respectively, represent the effectively coherent and dissipative coupling strengths between two modes. Note that the coherent coupling strength J arises from the mediation of the traveling wave, rather than the direct mode overlap of the two modes in a previous work [20]. At the separation of $L = 47$ mm, both J and Γ vanish, because γ is zero. J stays positive for all separations, but Γ would change sign at

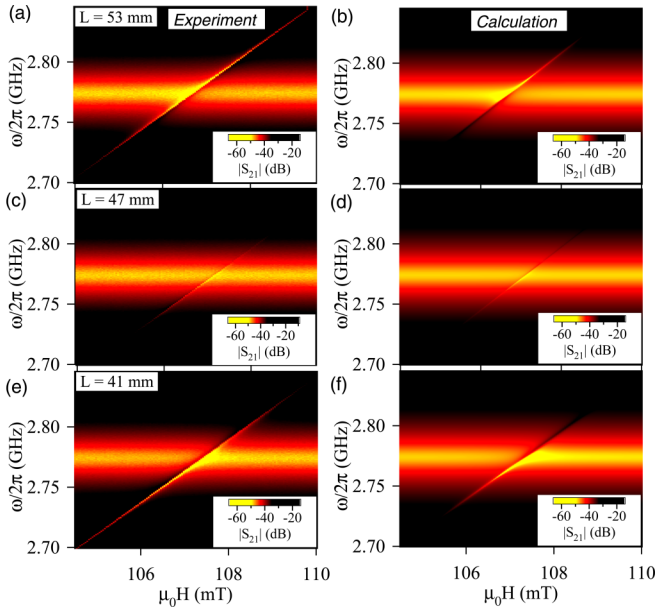

FIG. 4. Typical transmission mappings at three positions. (a), (c), and (e) Experimental results, respectively, measured at $L = 53$ mm, $L = 47$ mm, and $L = 41$ mm. Correspondingly, (b), (d), and (f) are the calculation results.

$L = 47$ mm. The switching sign of Γ results in the observed ultrasharp dip in transmission spectra changes from $-\Delta_a$ to $+\Delta_a$ [20].

C. Mode hybridization at different bias magnetic field

To further understand the interaction behaviors between two separated modes, we have chosen three separations and measured transmission spectra of the system with sweeping the bias magnetic field [Figs. 4(a), 4(c), and 4(e)]. From Figs. 4(a) and 4(e), a small gap occurs when frequencies of the two modes match with each other. In these two cases, coupling strengths $-i\sqrt{\kappa\gamma}e^{i\phi}$ are complex, so that mode hybridization of the system exhibits as a mixture of level repulsion and level attraction. By contrast, at the separation of $L = 47$ mm, because the radiative damping rate γ vanishes, coupling strength of the system decreases to almost zero. No obvious coupling gap can be observed in the transmission mapping [Fig. 4(c)]. Figures 4(b), 4(d), and 4(f) are calculation results based on our theoretical model. The consistency between experimental data and theoretical calculation demonstrates that our theory built on the mediation of traveling photons grasps the main features of the indirect interaction between a cavity photon mode and the magnon mode. Away from the cavity mode frequency, the difference between experimental data and calculations gradually emerges. The reason is that both ϕ and θ obtained at the condition of $\omega_a = \omega_m$ deviate from their actual values as $|\omega_a - \omega_m|$ increasing during calculations.

IV. CONCLUSION

In this work we studied the indirect interaction between a magnon mode and a cavity photon mode mediated by traveling photons. From a general Hamiltonian, we derived the effective coupling strength between two modes. It is determined by both values and the relative phase of the two modes' radiative damping rates, i.e., $-i\sqrt{\kappa\gamma}e^{i\phi}$. Therefore, at different separations, the coupling effect between them can be either coherent or dissipative. According to these theoretical predictions, we designed an experiment to test the interaction between a shield cavity photon mode and a magnon mode at different separations. Experimental observations confirm our theoretical predictions. Even without direct mode overlap, two modes can still couple with each other through their phase correlated dissipations into a mutual traveling photon bus. Our work demonstrates the indirect interaction mediated by traveling photons both in theory and experiment. The physics revealed in our work may help us develop the waveguide magnonics, and design new hybrid systems for quantum information processing.

ACKNOWLEDGMENTS

This work has been funded by NSERC (CA) Discovery Grants and NSERC Discovery Accelerator Supplements (C.-M.H.). J.W.R. is supported by CSC scholarship. We would like to thank Yutong Zhao and Pengchao Xu for discussions, and also acknowledge CMC Microsystems for providing equipment that facilitated this research.

[1] G. Khitrova, H. Gibbs, F. Jahnke, M. Kira, and S. Koch, Rev. Mod. Phys. **71**, 1591 (1999).
[2] J.-M. Raimond, M. Brune, and S. Haroche, Rev. Mod. Phys. **73**, 565 (2001).
[3] Z.-L. Xiang, S. Ashhab, J. Q. You, and F. Nori, Rev. Mod. Phys. **85**, 623 (2013).
[4] M. Aspelmeyer, T. J. Kippenberg, and F. Marquardt, Rev. Mod. Phys. **86**, 1391 (2014).
[5] G. Kurizki, P. Bertet, Y. Kubo, K. Mølmer, D. Petrosyan, P. Rabl, and J. Schmiedmayer, Proc. Natl. Acad. Sci. **112**, 3866 (2015).
[6] D. Lachance-Quirion, Y. Tabuchi, A. Gloppe, K Usami, and Y. Nakamura, Appl. Phys. Express **12**, 070101 (2019).
[7] Ö. O. Soykal and M. E. Flatté, Phys. Rev. Lett. **104**, 077202 (2010).
[8] H. Huebl, C. W. Zollitsch, J. Lotze, F. Hocke, M. Greifenstein, A. Marx, R. Gross, and S. T. B. Goennenwein, Phys. Rev. Lett. **111**, 127003 (2013).
[9] X. Zhang, C.-L. Zou, L. Jiang, and H. X. Tang, Phys. Rev. Lett. **113**, 156401 (2014).
[10] Y. Tabuchi, S. Ishino, T. Ishikawa, R. Yamazaki, K. Usami, and Y. Nakamura, Phys. Rev. Lett. **113**, 083603 (2014).
[11] M. Goryachev, W. G. Farr, D. L. Creedon, and Y. Fan, M. Kostylev, and M. E. Tobar, Phys. Rev. Appl. **2**, 054002 (2014).
[12] N. J. Lambert and J. A. Haigh, and A. J. Ferguson, J. Appl. Phys. **117**, 053910 (2015).

[13] L. Bai, M. Harder, Y. P. Chen, X. Fan, J. Q. Xiao, and C.-M. Hu, Phys. Rev. Lett. **114**, 227201 (2015).
[14] Y. Li, F. Zeng, S. Zhang, H. Shin, H. Saglam, V. Karakas, O. Ozatay, J. E. Pearson, O. G. Heinonen, and Y. Wu, A. Hoffmann, and W. Zhang, Phys. Rev. Lett. **122**, 117203 (2019).
[15] J. T. Hou and Luqiao Liu, Phys. Rev. Lett. **123**, 107702 (2019).
[16] X. Zhang, C.-L. Zou, N. Zhu, F. Marquardt, L. Jiang, and H. X. Tang, Nat. Commun. **6**, 8914 (2015).
[17] D. Lachance-Quirion, Y. Tabuchi, S. Ishino, A. Noguchi, T. Ishikawa, R. Yamazaki, and Y. Nakamura, Sci. Adv. **3**, e1603150 (2017).
[18] L. Bai, M. Harder, P. Hyde, Z. Zhang, C.-M. Hu, Y. P. Chen, and J. Q. Xiao, Phys. Rev. Lett. **118**, 217201 (2017).
[19] J. W. Rao, S. Kaur, B. M. Yao, E. R. J. Edwards, Y. T. Zhao, X. Fan, D. Xue, and T. J. Silva, Y. S. Gui, and C.-M. Hu, Nat. Commun. **10**, 2934 (2019).
[20] Y. P. Wang, J. W. Rao, Y. Yang, P. C. Xu, Y. S. Gui, B. M. Yao, J. Q. You, and C.-M. Hu, Phys. Rev. Lett. **123**, 127202 (2019).
[21] D. E. Chang, A. S. Sorensen, P. R. Hemmer, and M. D. Lukin, Phys. Rev. Lett. **97**, 053002 (2006).
[22] A. Gonzalez-Tudela, D. Martin-Cano, E. Moreno, L. Martin-Moreno, C. Tejedor, and F. J. Garcia-Vidal, Phys. Rev. Lett. **106**, 020501 (2011).
[23] E. Vetsch, D. Reitz, G. Sague, R. Schmidt, S. T. Dawkins, and A. Rauschenbeutel, Phys. Rev. Lett. **104**, 203603 (2010).
[24] A. Goban, K. S. Choi, D. J. Alton, D. Ding, C. Lacroute, M. Pototschnig, T. Thiele, N. P. Stern, and H. J. Kimble, Phys. Rev. Lett. **109**, 033603 (2012).
[25] A. F. Kockum, G. Johansson, and F. Nori, Phys. Rev. Lett. **120**, 140404 (2018).
[26] A. F. van Lool, A. Fedorov, K. Lalumière, B. C. Sanders, A. Blais, A. Wallraff, Science **342**, 1494 (2013).
[27] K. Lalumière, B. C. Sanders, A. F. van Loo, A. Fedorov, A. Wallraff, and A. Blais, Phys. Rev. A **88**, 043806 (2013).
[28] M. Mirhosseini, E. Kim, V. S. Ferreira, M. Kalaee, and A. Sipahigil, A. J. Keller, and O. Painter, Nat. Commun. **9**, 3706 (2018).
[29] M. Harder, Y. Yang, B. M. Yao, C. H. Yu, J. W. Rao, Y. S. Gui, R. L. Stamps, and C.-M. Hu, Phys. Rev. Lett. **121**, 137203 (2018).
[30] Vahram L. Grigoryan, K. Shen, and K. Xia, Phys. Rev. B **98**, 024406 (2018).
[31] A. Metelmann and A. A. Clerk, Phys. Rev. X **5**, 021025 (2015).
[32] Y. Yang, J. W. Rao, Y. S. Gui, B. M. Yao, W. Lu, and C.-M. Hu, Phys. Rev. Appl. **11**, 054023 (2019).
[33] W. Yu, J. Wang, H. Y. Yuan, and J. Xiao, Phys. Rev. Lett. **123**, 227201 (2019).
[34] J. W. Rao, C. H. Yu, Y. T. Zhao, Y. S. Gui, X. L. Fan, D. S. Xue, and C.-M. Hu, New J. Phys. **21**, 065001 (2019).
[35] B. Bhoi, B. Kim, S. H. Jang, J. Kim, J. Yang, Y. J. Cho, and S. K. Kim, Phys. Rev. B **99**, 134426 (2019).
[36] I. Boventer, M. Kläui, R. Macêdo, and M. Weides, New J. Phys. **21**, 125001 (2019).
[37] B. M. Yao, T. Yu, X. Zhang, W. Lu, Y. S. Gui, and C.-M. Hu, and Y. M. Blanter, Phys. Rev. B **100**, 214426 (2019).
[38] A. A. Clerk, M. H. Devoret, S. M. Girvin, Florian Marquardt, and R. J. Schoelkopf, Rev. Mod. Phys. **82**, 1155 (2010).
[39] D. F. Walls and G. J. Milburn, *Quantum Optics* (Springer, Berlin, 1994).
[40] C. W. Gardiner and M. J. Collett, Phys. Rev. A **31**, 3761 (1985).
[41] θ only affects the relative phase between two drive forces in Eq. (5), but has no influence on the effective coupling strength. In addition, because θ has no relation to the direction of input signal (p^{in}), it would not induce the nonreciprocity in our system.
[42] C. Hsu, B. Zhen, A. Stone, J. D. Joannopoulos, and M. Soljačić, Nat. Rev. Mater. **1**, 16048 (2016).
[43] Y. Yang, M. Harder, J. W. Rao, B. M. Yao, W. Lu, Y. S. Gui, and C.-M. Hu, AIP Adv. **8**, 075315 (2018).